The International Journal of Advanced Manufacturing Technology (2019) 101:1525–1536
https://doi.org/10.1007/s00170-018-3047-x

ORIGINAL ARTICLE

Analysis of tensile strength of a fused filament fabricated PLA part using an open-source 3D printer

Shilpesh R. Rajpurohit[1] · Harshit K. Dave[1]

Received: 10 July 2017 / Accepted: 15 November 2018 / Published online: 21 November 2018

Abstract

The application of the fused filament fabrication (FFF) or fused deposition modeling (FDM) may be limited due to relatively poor mechanical properties of the 3D-printed components. The present experimental investigation quantifies the effect of the three process parameters viz. raster angle, layer height, and raster width on the tensile properties of the FFF-printed PLA, using an open-source 3D printer. The mean effect of each process parameters on the tensile properties and the effect of the interaction are discussed. From the result analysis, it is found that raster angle, raster width, and interaction of layer height and raster width have a significant influence on the tensile properties. Tensile test results show that parts printed at 0° raster angle exhibit higher tensile strength as compared to those with 90° raster angle. Furthermore, fractography was performed on the tensile specimen using a high-precision measuring microscope to determine the effect of process variables on modes of failure. A close relationship between the raster angle and failure mode has been observed and critically discussed.

Keywords Fused filament fabrication (FFF) · Fused deposition modeling (FDM) · Polylactic acid (PLA) · Raster angle · Layer height · Raster width · Tensile strength

1 Introduction

Fused filament fabrication (FFF), widely known as fused deposition modeling (FDM), is one of the most widely used additive manufacturing techniques wherein parts can be built layer by layer through the extruded thermoplastic filament. FDM enables designer and engineers to develop a product using polymer material at low volume and low cost [1]. The raw material is in the form of a filament that is heated up to semi-solid state in liquefier head, then extruded through the heated nozzle to form a layer on the previously deposited layer. The newly deposited layer is solidified and adhered to the previously deposited layers due to diffusion bonding between layers. Eventually, it results in FDM part with any complex geometry [2]. FDM-built component can be considered as a laminated composite structure having vertically stacked layers of bonded rasters or beads. Because of that, mechanical properties of the FDM part are not only dependent on the quality of filament materials but are also dependent on the part orientation and raster angle that produces the anisotropic nature of properties.

FDM-fabricated parts are widely used in many industries like automobile, aerospace, medicine, electronics, customer product industries, etc. [3, 4]. FDM-produced parts have many promising applications even if they may be restricted due to relatively lower strength than that of the injection-molded part. Nowadays, FDM technique is applied for rapid manufacturing also, wherein the fabricated parts can be directly used as finished products. Therefore, it is required to have a detailed understanding of their associated mechanical properties for a better understanding of the behavior of FDM parts. The mechanical properties of the part must be sufficient so that it can meet the functional requirements.

With the growing application of 3D-printing technologies, a large number of polymer materials are being used for additive manufacturing. Polylactic acid (PLA) is one of the most widely used polymers in 3D-printing technologies. PLA is a biodegradable aliphatic polyester derived from lactic acid, extracted from sugar, cassava, corn starch, etc. [5]. PLA has excellent properties such as high strength and hardness, renewability, and low toxicity. However, certain properties of

✉ Harshit K. Dave
harshitkumar@yahoo.com

[1] Department of Mechanical Engineering, Sardar Vallabhbhai National Institute of Technology, Surat 395 007, India

PLA such as brittleness, low heat deflection temperature, poor crystallization, and narrow processing range limit its application [6]. Until now, few works have been reported to evaluate the mechanical properties of the 3D-printed PLA polymer. In addition, the recent upsurge in oil prices and significant advances in polymerization techniques for PLA have led to increase in price competitiveness relative to other polymers. Replacing petroleum-based polymer with PLA can reduce the consumption of petroleum-based resource and improve the eco-friendliness of the material [7, 8]. Increasing the content of a renewable resource in 3D-printed industries may also help to overcome the trade barriers caused by the environmental regulations. As PLA is relatively inexpensive, alternatives are also cost-effective. In recent time, various researchers have reported some research work to understand the mechanical properties of FDM-produced parts.

Liu et al. [9] applied the gray Taguchi method in order to optimize the mechanical properties of 3D-printed PLA part. They observed that orientation and layer height are significant for tensile strength, flexural strength, and impact strength. Cwikla et al. [10] investigated the effect of process parameters on the tensile strength of FDM printed ABS part using a DIY 3D printer. They found that higher tensile strength obtained at larger shell thickness and extrusion multiplier should always be above 0.9. Lanzotti et al. [11] studied the effect of layer thickness, infill orientation, and a number of shell perimeter on tensile properties of PLA part fabricated with Rep Rap Prusa i3 open-source 3D printer. They observed that as the infill orientation approaches to 90°, tensile strength decreases and it increases with increment in a number of perimeters. Malenka et al. [12] suggested using a higher level of percentage infill, maximizing part strength. Durugan et al. [13] reported part fabricated with 0° raster angle in the horizontal plane displayed higher mechanical properties. Riddick et al. [14] investigated the effect of build direction and raster angle on the tensile strength of the ABS part. Higher tensile strength has been obtain at 0° raster angle followed by ± 45°, 0°/90°, and 90° for horizontal and side build direction. The vertically built specimen shows the lowest tensile strength. Dawoud et al. [15] studied improvement in the mechanical properties of FDM specimen as compared to injection-molded parts. They suggested that negative raster gap along with ± 45° raster angle improves tensile and impact strength while 0°/90° improves flexural strength. Hill et al. [16] developed failure mechanism map that acquired effect of raster angle on the tensile strength of FDM part. They stated lower tensile strength and elongation to failure has been observed when the failure is resulting due to the bonding of beads rather than the beads. Ziemian et al. [17] studied the anisotropic tensile behavior of FDM-fabricated ABS part. They found that higher tensile strength has been obtained at 0° raster angle followed by ± 45°, 45°, and 90° raster angle. Ahn et al. [18] studied the anisotropy in properties of ABS part fabricated by FDM. They found that air gap and raster angle is the most significant parameter affecting the tensile strength of FDM part. Huang et al. [19] noted that tensile strength is gradually decreasing with increasing raster angle. Elastic modulus is also found to be decreased with increasing raster angle. Es Said et al. [20] reported that 0° raster angle has higher tensile strength than that observed at 90°. Anisotropy in the mechanical properties has been observed due to weak interlayer bonding and interlayer porosity. Vega et al. [21] observed that longitudinally built specimen had higher mechanical properties viz., tensile strength, flexural strength, and impact strength than the transversely built specimen. Chockalingam et al. [22] used a genetic algorithm to optimize process parameters to build a part with high tensile strength and density. Cantrell et al. [23] employed digital image correlation to evaluate the tensile and shear properties of 3D-printed ABS part. They found that raster angle and build orientation had a negligible effect on the tensile modulus. Sood et al. [24] studied the effect of layer thickness, orientation, raster angle, raster width, and air gap on the mechanical properties of ABS part. They observed that lower layer height, smaller raster angle, thicker raster, and zero gap improve the mechanical properties. Casavola et al. [25] did a comparative study of mechanical properties of PLA and ABS material and found that ABS has more orthotropic behavior than PLA. In addition to this, they also observed that when raster angle is shifted from 0° to 90°, tensile strength shows a reduction of 73.40% and 55.22% for ABS and PLA, respectively. Zaldivar et al. [26] reported that tensile properties of ULTEM 9085 specimen was significantly affected by build orientation. They achieved 46–85% of the reported tensile strength for the injection-molded specimen. Tymrak et al. [27] evaluated the mechanical properties of PLA and ABS materials fabricated by open-source 3D printer. They reported the tensile strength of 28.5 MPa and 56.6 MPa for ABS and PLA respectively, which is comparable with the tensile strength of the part fabricated by the commercial 3D printer. Rankouhi et al. [28] investigated the effect of layer thickness and orientation on the tensile properties of ABS part. They concluded that part fabricated with 0.2-mm-layer thickness has higher tensile strength than that printed with 0.4-mm-layer thickness. Wittbrodt et al. [29] studied the effect of color (i.e., white, black, blue, gray, and natural) and temperature on the mechanical properties of PLA part. They found that addition of color pigment can lower the tensile strength of the part and induce the percent crystallinity. White color filament had the highest percentage crystallinity at 210 °C temperature. Tanikella et al. [30] compared the tensile strength of commercially available various polymer filaments for 3D printing. They found that polycarbonate has the higher tensile strength (49 MPa) while HIPS has the lower tensile strength (19 MPa). Ninjaflex was found to be a most flexible material with an extension about 800%. Perez et al. [31] explored the effect of reinforcement on the tensile strength of FDM printed

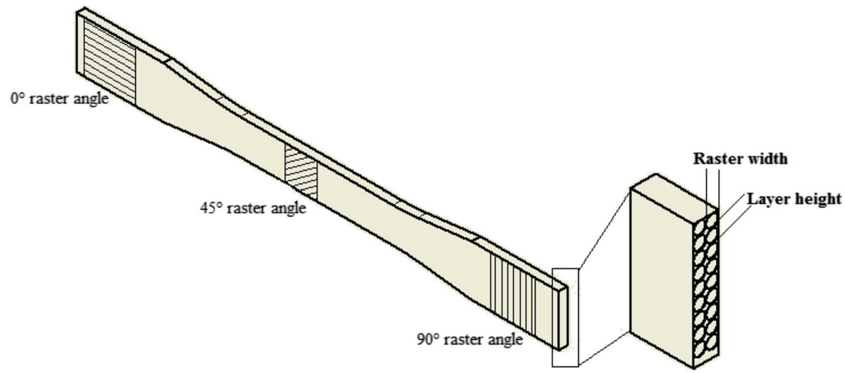

Fig. 1 Graphical representation of process parameters

ABS part. TiO_2 as reinforcement shows the higher tensile strength. They also found that addition of reinforcement displays the brittle fracture. The theoretical model proposed by Li et al. [32] suggests that higher stiffness of printed part can be obtained with negative air with raster deposited parallel to loading direction.

Until now, most of the research work has been carried out to study the effect of raster angle on the mechanical properties of ABS part. To the best of authors understanding, very less work has been reported to explore the effect of raster width and layer height on the mechanical properties of FDMed PLA part. It is required to study the effect of process parameters on the mechanical properties of 3D-printed PLA part so that it can meet the functional requirements. Initially, the authors fabricated rectangular-shaped PLA part and observed a significant effect of part orientation and fill density on the dimensional accuracy [33]. In the present study, the impact of the process parameters viz. layer height, raster angle, and raster width have been investigated on the PLA part fabricated using an open-source 3D printer. The purpose of the present study is to improve the knowledge about optimum parameter settings for printing functional PLA parts.

2 Experimental details

All the tensile specimens were built by using an OMEGA dual extruder open-source FDM printer. The machine has a build chamber of 500 mm × 500 mm × 500 mm with 100-μm-layer resolution. The printer has a positional accuracy of 11 μm in *x*-*y*-axis and 10 μm in *z*-axis with a nozzle diameter of 0.4 mm. It is capable to deposit material with a maximum speed of 150 mm/s. The printer is capable of printing with PLA, ABS, nylon, and PVA filament of 1.75 mm diameter.

The tensile strength of the FDM part is significantly affected by the selection of process parameters. Hence, in the

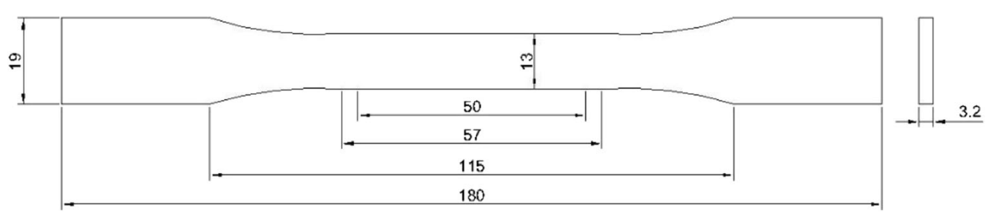

Fig. 2 Tensile specimen according to ASTM D638 (all dimensions are in mm)

Table 1 Process parameters and their levels

Fixed process parameters			Variable process parameters				
Parameters	Value	Unit	Parameters	Levels			Unit
				1	2	3	
Liquefier temperature	210	°C	Raster angle (RA)	0	45	90	°
Bed temperature	70	°C	Layer height (LH)	100	200	300	μm
Scan speed	50	mm/s	Raster width (RW)	500	600	700	μm
No. of perimeters	1	–					
% infill	100	%					
Infill pattern	Rectilinear	–					

Table 2 Typical properties of PLA material (Lanzotti et al. [11])

Physical	Nominal value
Specific gravity (23 °C)	1.24 to 1.26 g/cm^3
Melt mass-flow rate (MFR)	
210 °C/2.16 kg	6.0 to 78 g/10 min
190 °C/2.16 kg	1.5 to 36 g/10 min
Molding shrinkage	
Flow 73 °F	3.7E-3 to 4.1E-3 mm/mm
73 °F	0.30 to 1.1%
Mechanical	Nominal value
Tensile modulus (23 °C)	2020 to 3550 MPa
Tensile strength yield (23 °C)	15.5 to 72 MPa
Tensile strength break (23 °C)	14 to 70 MPa
Tensile elongation yield (23 °C)	9.8 to 10%
Tensile elongation break (23 °C)	0.50 to 9.2%
Flexural modulus (23 °C)	2392 to 4930 MPa
Flexural strength (23 °C)	48 to 110 MPa

present study, three process parameters viz., raster angle, layer height, and raster width have been selected for investigation on tensile strength, each at the three levels. The process parameters of FDM can be defined as follows:

(a) Raster angle—it is an inclination of the raster with respect to the *x*-axis of build table.
(b) Layer height—it is a thickness of the layer deposited by the nozzle.
(c) Raster width—it is a bead width, deposited as raster pattern used to fill interior region of the part.

Figure 1 shows the graphical representation of process parameters.

The entire tensile specimen has been designed and fabricated according to ASTM D638 standard. Figure 2 represents the schematic diagram of tensile specimen wherein dimension and geometry of test specimen can be seen. Pro-Engineering CAD software has been used to model the test specimen and

Table 3 Ultimate tensile strength and strain at break obtained from the full factorial experimental run

Sr. no.	Raster angle (°)	Layer height (μm)	Raster width (μm)	UTS (MPa)		Strain at break (ε_f)	
				Mean	SD	Mean	SD
1.	0	100	500	44.50	2.26	8.87	1.47
2.	0	100	600	47.30	2.69	9.99	4.26
3.	0	100	700	45.65	3.04	9.18	2.80
4.	0	200	500	42.20	0.85	8.07	2.83
5.	0	200	600	45.70	0.57	8.46	3.56
6.	0	200	700	43.50	0.42	6.58	0.72
7.	0	300	500	46.65	1.20	11.12	6.02
8.	0	300	600	38.50	3.54	5.19	0.17
9.	0	300	700	39.35	1.91	5.15	0.28
10.	45	100	500	24.49	0.40	5.91	1.35
11.	45	100	600	45.15	1.48	6.69	0.08
12.	45	100	700	38.25	1.48	6.13	0.40
13.	45	200	500	32.95	1.48	6.07	0.32
14.	45	200	600	35.30	4.10	6.64	0.64
15.	45	200	700	34.45	0.35	5.94	0.51
16.	45	300	500	36.30	4.67	6.39	2.61
17.	45	300	600	30.95	4.02	6.41	0.16
18.	45	300	700	31.55	1.77	6.47	0.87
19.	90	100	500	21.94	0.35	4.76	0.27
20.	90	100	600	40.45	3.04	5.78	0.42
21.	90	100	700	34.00	2.69	5.57	0.72
22.	90	200	500	26.35	3.32	5.16	0.35
23.	90	200	600	35.00	3.96	5.58	0.25
24.	90	200	700	31.70	0.57	5.63	0.46
25.	90	300	500	34.10	0.99	5.83	1.62
26.	90	300	600	34.50	1.41	5.59	0.52
27.	90	300	700	26.75	4.74	5.49	0.51

Fig. 3 Test specimen after tensile testing

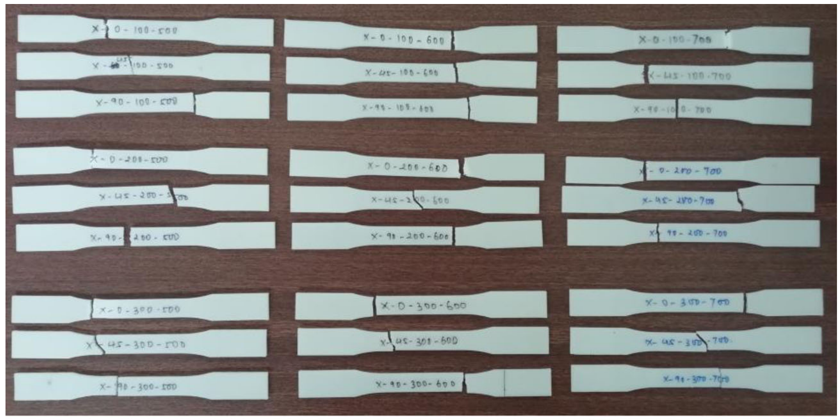

Trial set 1

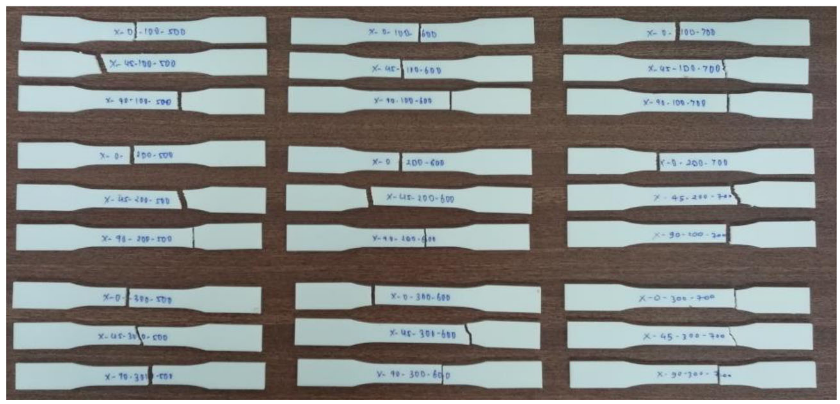

Trial set 2

saved as an STL file. The STL file is then imported into Repetier host software with Slice3r as slicer engine (open-source 3D printer software). The Repetier host has been used to control the printer setting, such as layer height, percentage infill, part orientation, scan speed, etc. Finally, a .gcode file was generated and transferred to the OMEGA dual extruder printer to fabricate the 3D specimen. All the variable process parameters (as shown in Fig. 1) were controlled using Repetier host software. Table 1 shows the fixed and variable process parameters during printing of tensile specimen.

Tensile specimen as shown in Fig. 2 was manufactured using 1.75 mm diameter PLA (polylactic acid) filament. The

Fig. 4 Main effect of process parameters on tensile strength

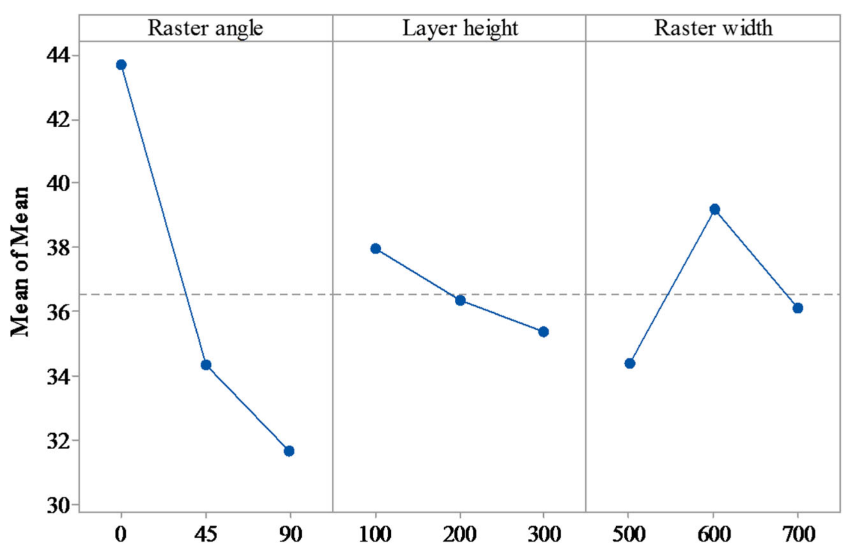

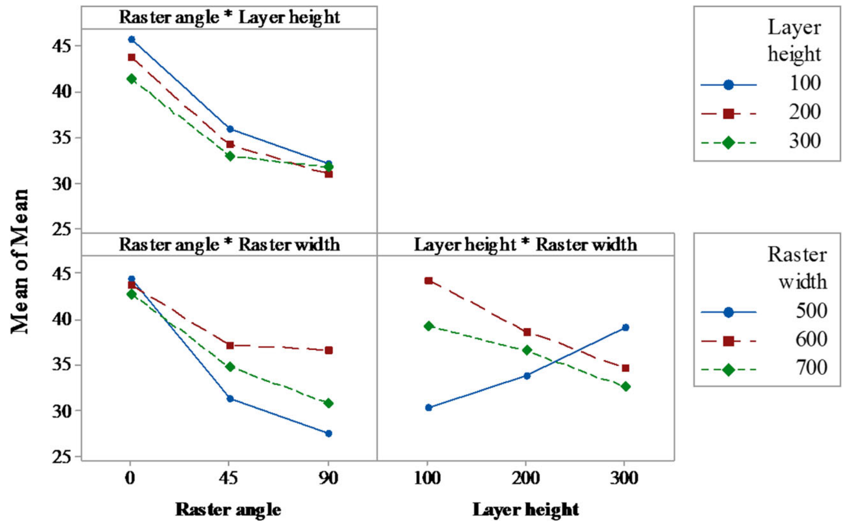

Fig. 5 Interaction effect of process parameters on tensile strength

same brand of the PLA filament spool has been used to fabricate specimen so that same properties of filament material can be assured. Table 2 shows the typical properties of PLA material.

Tinius Olsen H50KL tensile testing machine has been used to perform a tensile test on the test specimen. The machine was equipped with 50-kN load cell and built-in Horizon software allows to control, monitor, and record the measurement data. Test samples were tested until failure at a crosshead speed of 5 mm/min. Test data such as force and grip displacement were recorded through the Horizon software. After the tensile test, the fractured surface has been microscopically examined by using the high-precision measuring microscope (Sipcon SDM TRZ-5300) which has a magnification range from × 35 to × 225.

In the present investigation, the full factorial design has been used to perform an experimental run at every combination of the factor levels. Three factors have been varied at the three levels so according to full factorial experimental design, total 27 number of experiments need to be performed as shown in Table 3. Two identical test specimens are built for each experimental run, which resulted in a total of 54 test specimens for full factorial experimental design. For each experiential run, the process parameters were set according to full factorial experimental design.

3 Results and discussion

The tensile test was performed to measure the effect of different raster angle, layer height, and raster width on the 3D-printed part. All the experiments were performed as per the experimental plan as discussed. Figure 3 shows all the broken test specimens after tensile testing.

Main effect plots are constructed using the mean of each parameter at all the levels. The maximum values of mean for parameters together become the optimal combination of parameters. The significance of each parameter on tensile

Table 4 Analysis of variance (ANOVA) for tensile strength

Source	DF	SS	MS	*F*-value	*p* value	Contribution
Model	18	1245.03	69.168	8.75	0.002	95.17%
Linear	6	857.42	142.904	18.09	0.000	65.54%
Raster angle	2	719.99	359.995	45.56	0.000	55.03%
Layer height	2	30.25	15.126	1.91	0.209	2.31%
Raster width	2	107.18	53.591	6.78	0.019	8.19%
2-way interactions	12	387.61	32.301	4.09	0.027	29.63%
Raster angle×layer height	4	13.52	3.38	0.43	0.785	1.03%
Raster angle×raster width	4	79.15	19.786	2.5	0.125	6.05%
Layer height×raster width	4	294.95	73.736	9.33	0.004	22.55%
Error	8	63.21	7.902			4.83%
Total	26	1308.25				

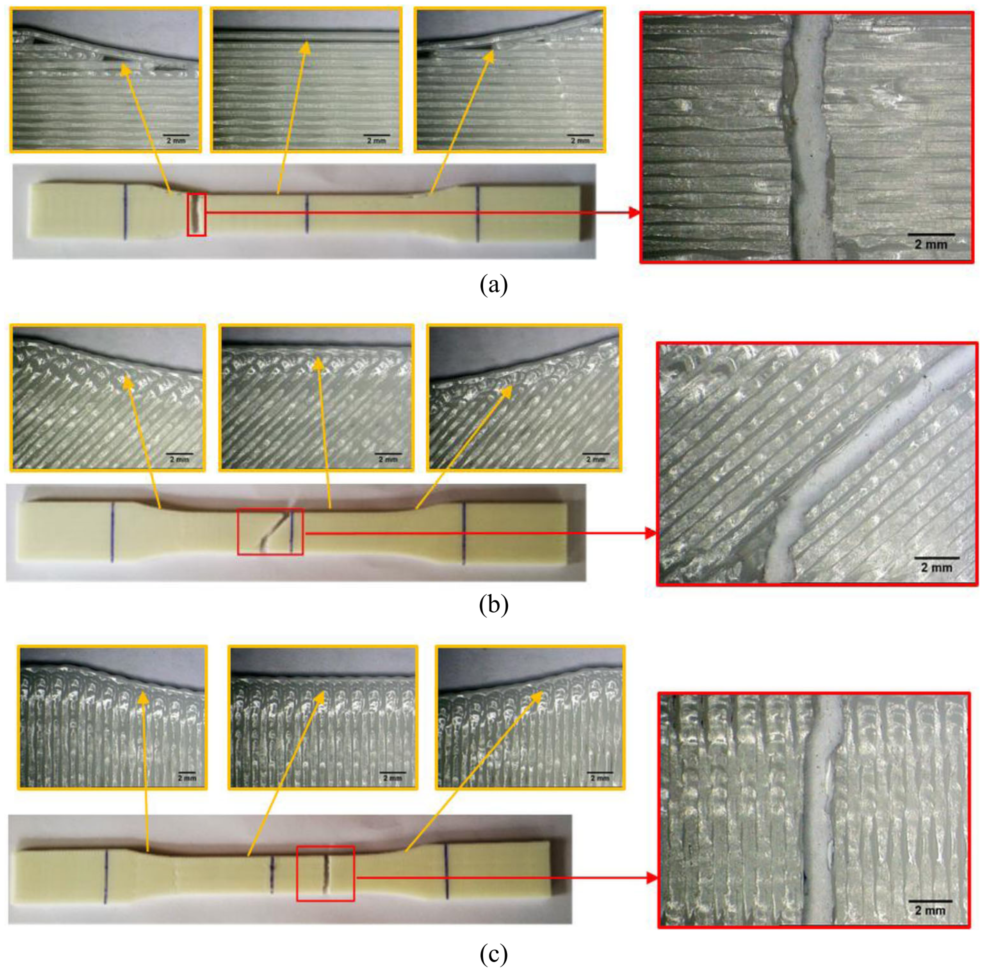

Fig. 6 Fracture images of the specimen after tensile testing at **a** 0°, **b** 45°, and **c** 90° raster angle (× 35 magnification)

strength is obtained by analyzing the observation through analysis of variance (ANOVA). The analysis showed the main and interaction effects of the process parameters on the tensile strength. The main effect is the direct effect of independent parameters while interaction effect is the joint effect of two independent parameters on tensile strength. Figure 4 shows the main effect plot of process parameters on the tensile strength of FDM specimen. It can be seen that tensile strength decreases with increase in raster angle and layer height and increases with increase in raster width up to 600 μm. The analysis of mean reveals that the optimal performance for tensile strength can be obtained at raster angle 0° (level 1), layer height 100 μm (level 1), and raster width 600 μm (level 2). Analysis of mean also reveals that raster angle has the strong effect on tensile strength followed by raster width and layer height.

The interaction effect of parameters is shown in Fig. 5 and it represents an average of mean to all possible combinations of any two factors. If two lines intersect, then there is a possible interaction between these two factors. From Fig. 5, it is clear that there is a strong interaction between layer height and raster width, whereas no interaction is observed between other factors combinations. When the layer height is set to 100 μm, it results in higher tensile strength at all levels for other factors. At the 100-μm-layer height, higher tensile strength is observed with 600-μm-raster width. However, when the layer height increased to 300 μm, higher tensile strength is observed with 500-μm-raster width. When layer height and raster width are set at higher values simultaneously, there is a possibility of generation of voids that reduce the tensile strength. It can be stated from Fig. 5 that at higher layer height, smaller raster width may be preferred to obtain maximum tensile strength.

Further, it is necessary to find out the parameter that significantly affects the tensile strength of specimen. It has been also carried out to identify most significant parameters in terms of in percentage affecting the response parameter through ANOVA (analysis of variance). The p value represents the statistical importance of individual parameters. It was stated by Taguchi et al. [34] that the p value should be less than 0.05 for the 95% confidence level. The ANOVA result for mean data of tensile strength is given in Table 4.

From Table 4, it can be observed that p value of raster angle and raster width is lesser than 0.05. However, only one interaction between layer height and raster width has been lesser

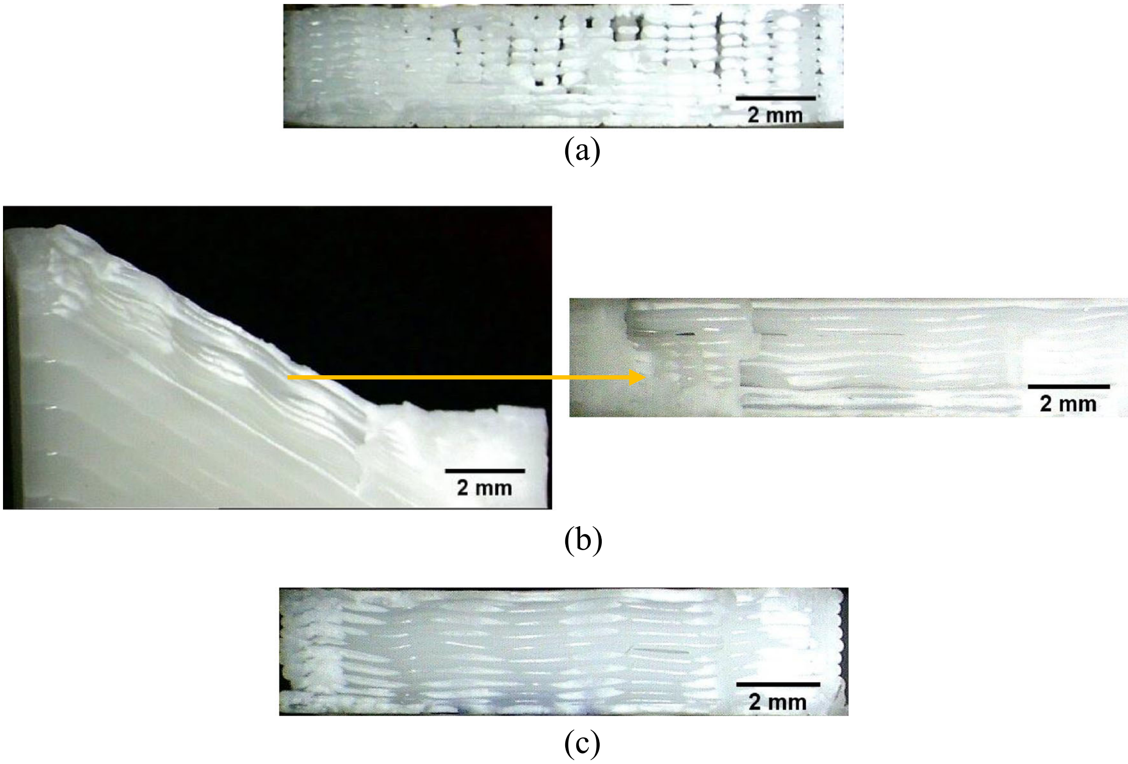

Fig. 7 Microscopic examination of the fractured surface at **a** 0°, **b** 45°, and **c** 90° raster angle (× 35 magnification)

than 0.05. Hence, these factors have a statistically significant effect on tensile strength at the 95% confidence interval. Subsequently, raster angle is the most significant parameter affecting tensile strength followed by the interaction between layer height and raster width (22.55%) and raster width (8.19%).

3.1 Effect of raster angle

From the ANOVA (as shown in Table 4), it is found that *p* value of raster angle is less than the 0.05, hence raster angle is significant at 95% confidence interval. Further, it can be seen from Fig. 4, as the raster angle increases from 0° to 90°, tensile strength has been decreased. It may be due to at 0° raster angle, all the layers have been deposited parallel to the loading direction of tensile strength. Due to the parallel alignment of layers and loading direction, individual layers capable to bear more load during tensile testing as well the effect of raster bonding also minimized. At 0° raster angle, higher ductility has been also observed, it may be due to all the fibers that are orientated along the loading direction. In this condition, the specimen shows the higher stiffness, as each fiber takes the load and the effect of the raster to raster bonding is minimized. While at 90°, lowest tensile strength has been obtained due to the perpendicular alignment of layers to the loading direction. Due to the perpendicular alignment of layers to the loading direction, the strength of fabricated part is dependent on the bonding strength between adjacent rasters and it has been always less than that of the continuous deposition. At 45°, tensile strength has been found in between 0° and 90° raster angle, where layers have been deposited at 45° to the loading direction. Tensile strength at 45° raster angle is dependent on the shear strength of adjacent rasters. The strain at break was found to be least with 90° raster angle. At 90° raster angle, all the rasters are orientated perpendicular to the loading direction. In this condition, the specimen shows the lowest stiffness, as load taken by the bonding between the rasters, which is weakened compared to monofilament results into brittle failure with low stiffness. Raster angle does not have any significant interaction with layer height and raster width. Apparently, higher tensile strength has been obtained at 0° raster angle irrespective of layer height and raster width.

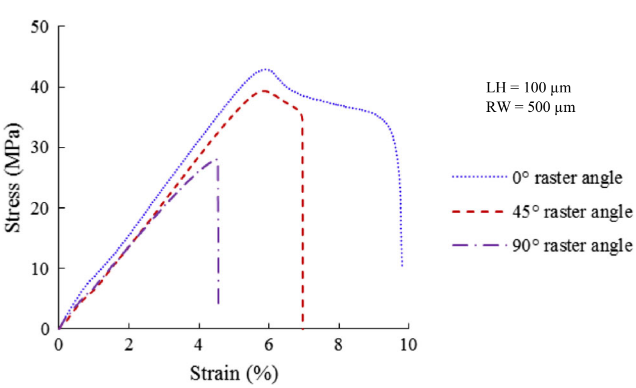

Fig. 8 Stress-strain curve for different raster angle at 100-µm-layer height and 500-µm-raster width

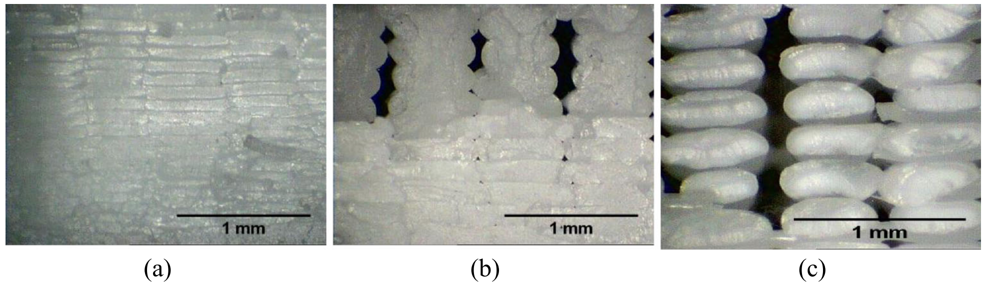

Fig. 9 Fracture images of the specimen after tensile testing at **a** 100-μm, **b** 200-μm, and **c** 300-μm-layer height (× 200 magnification)

Figure 6 shows the fractured image of the tensile specimen at different raster angle. Figure 6 also shows that mode of fracture is highly dependent on raster deposition angle. For 0° raster angle, it can be seen that fracture has occurred perpendicular to deposition direction with a significant amount of ductility. As the raster angle is increased to 45°, fracture takes place along the raster deposition direction that is along with 45°. For 90° raster angle, the fracture is observed through bonding of adjacent rasters and brittle fracture is observed with a loss of ductility. There has been a chance of premature failure of the specimen during testing because of accumulated stress concentration at fillet areas as shown in Fig. 6. This stress concentration is mainly due to raster termination near the fillet radius as shown by the arrow in Fig. 6. This type of failure pattern near the fillet area has been also observed and reported by different researchers [2, 16, 18, 35, 36].

Figure 7 shows the failure surface of the specimen with respect to raster angle. It can be seen that with 0° raster angle failure is mainly associated with failure of raster itself, which results in higher tensile strength. It is also observed that fracture takes place due to the breaking of individual rasters. There is a significant amount of pulling and necking of individual raster can be observed. On the other hand, for a specimen with 45° and 90° raster angle, brittle failure has been observed because of failure occurs mainly through bonding of adjacent rasters and delamination or separation of raster occurs. Bonding of raster is always significantly weaker than raster that results in lesser tensile strength.

The increment in raster angle from 0° to 90° also shifts the mode of failure from ductile failure to brittle failure as shown in Fig. 8. As shown in Fig. 8, a specimen with 0° raster angle exhibits 9.92% elongation while 4.57% elongation has been observed in 90° raster angle, which clearly indicates the shifting mode of failure from ductile to brittle.

3.2 Effect of layer height

From the ANOVA (as shown in Table 3), it is found that *p* value of layer height is greater than the 0.05; hence, layer height is not considered statistically significant at 95% confidence interval. Further, it can be observed from Fig. 4 that as the layer height increases, tensile strength decreases. Higher

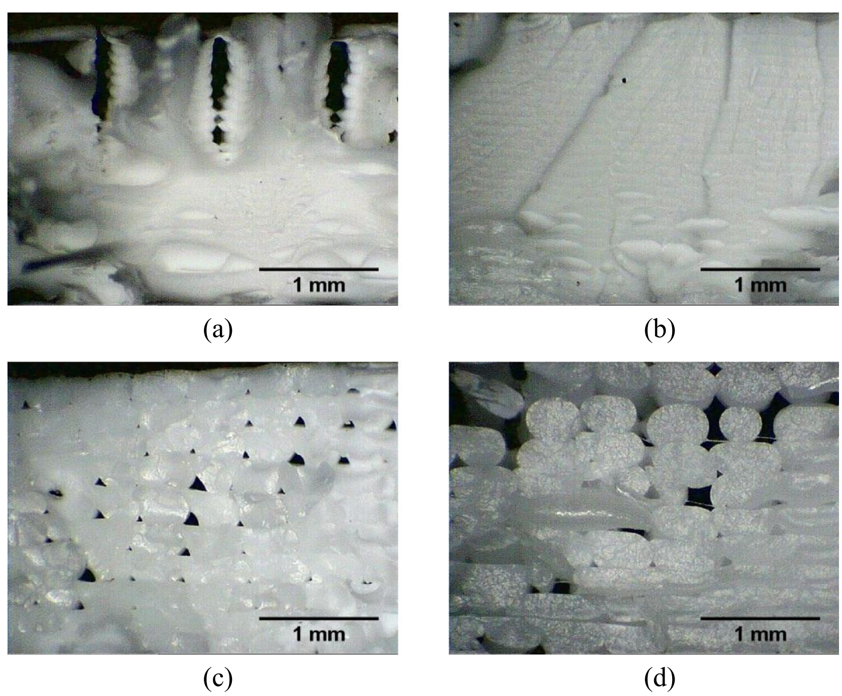

Fig. 10 Fracture surface of specimen after tensile test at **a** 100-μm-layer height and 500-μm-raster width, **b** 100-μm-layer height and 600-μm-raster width, **c** 300-μm-layer height and 500-μm-raster width, and **d** 300-μm-layer height and 600-μm-raster width (× 150 magnification)

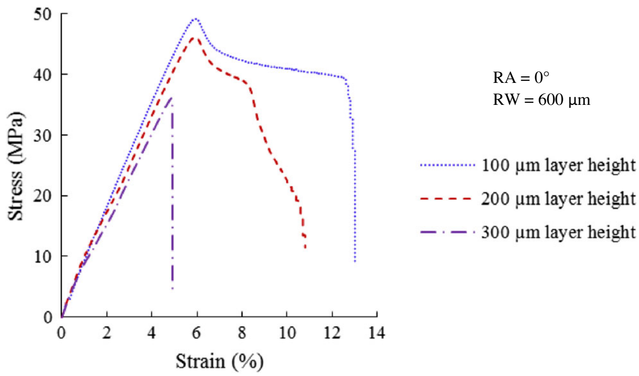

Fig. 11 Stress-strain curve for different layer height at 0° raster angle and 600-μm-raster width

tensile strength has been observed at the minimum layer height. It may be because lower value of layer height gives higher bonding area between layers those results into the greater bonding strength between layers. Higher stiffness is also obtained at lower layer height because of higher bonding area among rasters that give the capability to withstand more load comparatively. As the layer height increases, the bonding area between adjacent layers decreases resulting in a decrease in bonding strength between layers. Figure 9 shows the fractured surface of the tensile specimen at different values for layer height. Similarly, it can be seen from Fig. 9, at lower layer height, higher bonding region can be observed between the adjacent layers while lesser bonding area can be observed at the higher value of layer height due to the presence of voids. The reduced bonding area between adjacent layers is resulting in lower tensile strength at higher layer height. These results are found to be in good agreement with the observation reported by Coogan et al. [37]. At lower layer height, higher extrusion pressure may help layers to form a quick and intimate bond, which results in greater bond strength. Similarly, low stiffness and low strain at break have been observed at higher layer height, and the presence of voids and reduced bonding area among rasters leads to brittle failure.

As mentioned in Table 4, the interaction between layer height and raster width is found to be significant with a contribution of 22.55% on the response. From the main effect plot (as shown in Fig. 4), it can be seen that higher tensile strength is observed at 100-μm-layer height. It can be seen from Fig. 4, higher tensile strength has been observed at 100-μm-layer height at all values for raster width and maximum tensile strength has been observed with 600-μm-raster width. On the other hand, as the layer height approaches to 300 μm, maximum tensile strength has been obtained at 500-μm-raster width. Referring to the images in Fig. 10, it is noted that at 100-μm-layer height and 600-μm-raster width, fewer voids have been observed and higher necking is observed between the adjacent raster. While keeping raster width constant at 600 μm and increasing layer height in increased to 300 μm (Fig. 10d), a number of voids have been observed with less amount of necking between rasters. On the other hand, at 300-μm-layer height, reduction in raster width to 500 μm enhances the necking phenomena and reducing the voids (Fig. 10c).

Figure 11 shows the stress-strain curve for different layer height. It can be seen that from the stress-strain curve at 100-μm-layer height, higher tensile strength of 49.2 MPa with a significant amount of elongation of 13% while at 300-μm-layer height lower tensile strength of 36 MPa has been obtained with 5.07% elongation. It is also evident that at higher layer height, mode of failure transits for ductile failure to brittle failure with a loss ductility. It may be due to that there is a presence of voids because of smaller bonding area between layer interfaces at higher layer height and voids can be the reason for easy crack initiation and propagation in the specimen resulting into abrupt failure. This abrupt failure leads to brittle failure with lower tensile strength at higher layer height.

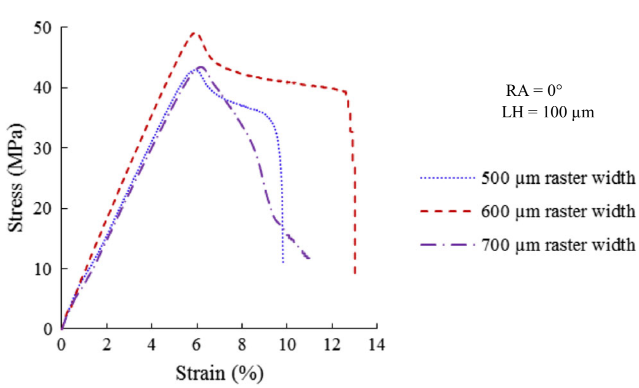

Fig. 12 Stress-strain curve for different raster width at 0° raster angle and 100-μm-layer height

3.3 Effect of raster width

From the ANOVA (as shown in Table 3), it is found that *p* value of raster width is less than the 0.05; hence, raster width is statistically significant at 95% confidence interval. It can be seen from Fig. 4 that with an increase in raster width, tensile strength also increases up to 600-μm-raster width and then it decreases as the raster width is increased. Further, at higher raster width, raster possesses higher thermal energy because of which cooling takes longer time and hence, raster remains above glass transition temperature for longer time. This allows improving the bonding area between layer interfaces resulting in greater strength. The larger raster width with improving adhesion between layers results in higher bond strength. Coogan et al. [37] have reported a similar observation. It can be also noted that at 700-μm-raster width, tensile strength has been less compared to 600-μm-raster width, which may be due to the presence of voids between the layers. Similarly, higher stiffness has been observed with the 600-μm-raster width then after it starts decreasing.

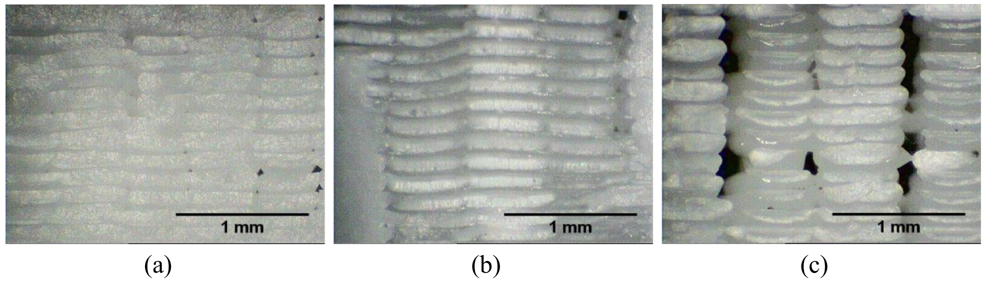

Fig. 13 Fracture images of the specimen after tensile testing at **a** 500 μm, **b** 600 μm, and **c** 700-μm-raster width (× 200 magnification)

Figure 12 shows the stress-strain curve for different raster width. From Fig. 12, it can be seen that higher tensile strength (49.2 MPa) has been obtained at 600-μm-raster width with an elongation of 13%. As the raster width is increased from 600 to 700 μm, it is observed that tensile strength is decreased from 49.2 to 43.5 MPa with a 14% reduction in elongation. Thus, it is evident that as the raster width is increased, tensile strength also increases up to a certain extent after which its start decreasing. From Fig. 13, it can be seen that at 500- and 600-μm-raster width, the bonding area between adjacent layers is larger compared to that at 700-μm-raster width, where bonding area between the adjacent layers is lesser and presence of voids can also be seen. Presence of voids can act as a stress concentrator between layers, due to which crack may be easily initiated and propagated ultimately resulting in lower tensile strength at 700-μm-raster width. Due to the presence of voids, effective cross-section area has been also reduced that can also be the reason for reduced tensile strength at 700-μm-raster width.

4 Conclusion

In the present study, the tensile properties of PLA specimen printed using an open-source 3D printer are characterized through a standard tensile test to determine the ultimate tensile strength and strain at break. These results indicate that specimens printed with open-source 3D printer are comparable in tensile strength to those of the specimens printed on a commercial 3D printer. The tensile properties of the specimen can be improved through the proper adjustment of the process variables.

Based on the analysis of the experimental results made, it was found that the parallel arrangement of the fibers to the loading direction obtained the higher tensile strength for parts printed with 0° raster angle. The larger bonding area at the lower layer height and higher raster width are resulting in the higher strength of the printing part. Microscopic examination of the part with 0° raster angle specimen shows the fiber discontinuity and voids in the fillet region, which may be the reason for the premature failure of the part. Furthermore, voids have also been observed on the cross-section of the printed PLA, which indicates a low degree of diffusion among layers and rasters that results into brittle failure.

References

1. Bikas H, Stavropoulos P, Chryssolouris G (2016) Additive manufacturing methods and modelling approaches: a critical review. Int J Adv Manuf Technol 83(1–4):389–405
2. Garg A, Bhattacharya A, Batish A (2017) Chemical vapor treatment of ABS parts built by FDM: analysis of surface finish and mechanical strength. Int J Adv Manuf Technol 89(5–8):2175–2191
3. Jin YA, He Y, Xue GH, Fu JZ (2015) A parallel-based path generation method for fused deposition modeling. Int J Adv Manuf Technol 77:927–937
4. Kuo CC, Chen CM, Chang SX (2017) Polishing mechanism for ABS parts fabricated by additive manufacturing. Int J Adv Manuf Technol 91(5–8):1473–1479
5. Pivsa-Art W, Chaiyasat A, Pivsa-Art S, Yamane H, Ohara H (2013) Preparation of polymer blends between poly (lactic acid) and poly (butylene adipate-co-terephthalate) and biodegradable polymers as compatibilizers. Energy Procedia 34:549–554
6. Zhang J, Wang S, Qiao Y, Li Q (2016) Effect of morphology designing on the structure and properties of PLA/PEG/ABS blends. Colloid Polym Sci 294(11):1779–1787
7. Choe IJ, Lee JH, Yu JH, Yoon JS (2014) Mechanical properties of acrylonitrile–butadiene–styrene copolymer/poly (l-lactic acid) blends and their composites. J Appl Polym Sci 131(11):40329.1–40329.8
8. Jo MY, Ryu YJ, Ko JH, Yoon JS (2012) Effects of compatibilizers on the mechanical properties of ABS/PLA composites. J Appl Polym Sci 125(S2):E231–E238
9. Liu X, Zhang M, Li S, Si L, Peng J, Hu Y (2017) Mechanical property parametric appraisal of fused deposition modeling parts based on the gray Taguchi method. Int J Adv Manuf Technol 89(5–8):2387–2397
10. Cwikła G, Grabowik C, Kalinowski K, Paprocka I, Ociepka P (2017) The influence of printing parameters on selected mechanical properties of FDM/FFF 3D-printed parts. IOP Conf Ser Mater Sci Eng 227(1):012033
11. Lanzotti A, Grasso M, Staiano G, Martorelli M (2015) The impact of process parameters on mechanical properties of parts fabricated in PLA with an open-source 3-D printer. Rapid Prototyp J 21(5):604–617
12. Melenka GW, Schofield JS, Dawson MR, Carey JP (2015) Evaluation of dimensional accuracy and material properties of the MakerBot 3D desktop printer. Rapid Prototyp J 21(5):618–627
13. Durgun I, Ertan R (2014) Experimental investigation of FDM process for improvement of mechanical properties and production cost. Rapid Prototyp J 20(3):228–235
14. Riddick JC, Haile MA, Von Wahlde R, Cole DP, Bamiduro O, Johnson TE (2016) Fractographic analysis of tensile failure of

acrylonitrile-butadiene-styrene fabricated by fused deposition modeling. Addit Manuf 11:49–59

15. Dawoud M, Taha I, Ebeid SJ (2016) Mechanical behaviour of ABS: an experimental study using FDM and injection moulding techniques. J Manuf Process 21:39–45
16. Hill N, Haghi M (2014) Deposition direction-dependent failure criteria for fused deposition modeling polycarbonate. Rapid Prototyp J 20(3):221–227
17. Ziemian S, Okwara M, Ziemian CW (2015) Tensile and fatigue behavior of layered acrylonitrile butadiene styrene. Rapid Prototyp J 21(3):270–278
18. Ahn SH, Montero M, Odell D, Roundy S, Wright PK (2002) Anisotropic material properties of fused deposition modeling ABS. Rapid Prototyp J 8(4):248–257
19. Huang B, Singamneni S (2015) Raster angle mechanics in fused deposition modelling. J Compos Mater 49(3):363–383
20. Es Said OS, Foyos J, Noorani R, Mendelson M, Marloth R, Pregger BA (2000) Effect of layer orientation on mechanical properties of rapid prototyped samples. Mater Manuf Process 15(1):107–122
21. Vega V, Clements J, Lam T, Abad A, Fritz B, Ula N, Es-Said OS (2011) The effect of layer orientation on the mechanical properties and microstructure of a polymer. J Mater Eng Perform 20(6):978–988
22. Chockalingam K, Jawahar N, Praveen J (2016) Enhancement of anisotropic strength of fused deposited ABS parts by genetic algorithm. Mater Manuf Process 31(15):2001–2010
23. Cantrell JT, Rohde S, Damiani D, Gurnani R, DiSandro L, Anton J, Young A, Jerez A, Steinbach D, Kroese C, Ifju PG (2017) Experimental characterization of the mechanical properties of 3D-printed ABS and polycarbonate parts. Rapid Prototyp J 23(4):811–824
24. Sood AK, Ohdar RK, Mahapatra SS (2010) Parametric appraisal of mechanical property of fused deposition modelling processed parts. Mater Des 31(1):287–295
25. Casavola C, Cazzato A, Moramarco V, Pappalettere C (2016) Orthotropic mechanical properties of fused deposition modelling parts described by classical laminate theory. Mater Des 90:453–458
26. Zaldivar RJ, Witkin DB, McLouth T, Patel DN, Schmitt K, Nokes JP (2017) Influence of processing and orientation print effects on the mechanical and thermal behavior of 3D-printed ULTEM® 9085 material. Addit Manuf 13:71–80
27. Tymrak BM, Kreiger M, Pearce JM (2014) Mechanical properties of components fabricated with open-source 3-D printers under realistic environmental conditions. Mater Des 58:242–246
28. Rankouhi B, Javadpour S, Delfanian F, Letcher T (2016) Failure analysis and mechanical characterization of 3D printed ABS with respect to layer thickness and orientation. J Fail Anal Prev 16(3):467–481
29. Wittbrodt B, Pearce JM (2015) The effects of PLA color on material properties of 3-D printed components. Addit Manuf 8:110–116
30. Tanikella NG, Wittbrodt B, Pearce JM (2017) Tensile strength of commercial polymer materials for fused filament fabrication 3D printing. Addit Manuf 15:40–47
31. Perez ART, Roberson DA, Wicker RB (2014) Fracture surface analysis of 3D-printed tensile specimens of novel ABS-based materials. J Fail Anal Prev 14(3):343–353
32. Li L, Sun Q, Bellehumeur C, Gu P (2002) Composite modeling and analysis for fabrication of FDM prototypes with locally controlled properties. J Manuf Process 4(2):129–141
33. Rajpurohit SR, Dave HK (2016) Parametric studies on quality of PLA parts produced using fused deposition modelling. In: Proceeding: 6th International & 27th All India Manufacturing Technology, Design and Research Conference (AIMTDR-2016), pp 59–62
34. Taguchi G, Chowdhury S, Wu Y (2005) Taguchi's quality engineering handbook. Wiley, Hoboken, p 1736
35. Torres J, Cole M, Owji A, DeMastry Z, Gordon AP (2016) An approach for mechanical property optimization of fused deposition modeling with polylactic acid via design of experiments. Rapid Prototyp J 22(2):387–404
36. Croccolo D, De Agostinis M, Olmi G (2013) Experimental characterization and analytical modelling of the mechanical behaviour of fused deposition processed parts made of ABS-M30. Comput Mater Sci 79:506–518
37. Coogan TJ, Kazmer DO (2017) Bond and part strength in fused deposition modeling. Rapid Prototyp J 23(2):414–422